SCIPEDIA

Surface Settlement of Small Clear Distance Tunnel in Soft Soil Layer during Shield Propulsion

Xun Zhao*, Shuangshuang Wu, Fuyu Jiang and Song Chen*

School of Earth Sciences and Engineering, Hohai University, Nanjing, 211100, China

INFORMATION

Keywords:
Small clear distance tunnel
shield method
numerical simulation
soil settlement law
double-line tunnel construction
comparative analysis

DOI: 10.23967/j.rimni.2025.10.65613

SCIPEDIA
Revista Internacional de Métodos Numéricos para Cálculo y Diseño en Ingeniería
RIMNI

Surface Settlement of Small Clear Distance Tunnel in Soft Soil Layer during Shield Propulsion

Xun Zhao*, Shuangshuang Wu, Fuyu Jiang and Song Chen*

School of Earth Sciences and Engineering, Hohai University, Nanjing, 211100, China

ABSTRACT

Shield tunneling has become a widely adopted method for urban underground transport construction. However, research on the impact of small-clearance shield tunnel construction in urban soft soil layers is still in its early stages. Understanding the effects of such construction on surface settlement and summarizing temporal settlement patterns is crucial for reducing construction risks and minimizing disturbances to the surrounding areas. This paper investigates the impact of two-lane small-clearance tunneling on surface settlement through finite element modeling and analysis, focusing on the Nanjing Heyan Road Crossing as a case study. The study also evaluates the feasibility of different construction distances in successive two-lane shield tunneling. Numerical simulations and on-site measurements were conducted to explore the surface settlement behavior under varying construction distances. The research examines the vertical and lateral settlement characteristics in the backfilled area, located 32 m from the tunnel initiation well. The findings reveal the settlement behavior throughout the shield tunneling process under different construction distances. The results indicate that the vertical settlement profiles of shield tunnel construction in soft soil layers conform to the Mindlin settlement curve, while the lateral settlement profiles follow the double-funnel Peck curves. Additionally, the closer the construction distance between the two tunnels, the greater the disturbance to the ground surface, whereas increasing the construction distance results in higher peak surface settlement. Soil settlement around the tunnel is significantly affected by construction disturbances, structural stiffness, lateral unloading bias, the extrusion effect of tube sheet weight, and shield machine movement. The use of synchronous grouting effectively mitigates excessive surface settlement. This study provides valuable insights and serves as a reference for similar shield tunnel construction projects in urban soft soil layers.

OPEN ACCESS

Received: 18/03/2025

Accepted: 16/05/2025

Published: 22/09/2025

DOI
10.23967/j.rimni.2025.10.65613

Keywords:
Small clear distance tunnel
shield method
numerical simulation
soil settlement law
double-line tunnel construction
comparative analysis

*Correspondence: Xun Zhao, Song Chen (zhaoxun2333@hotmail.com, chensong@hhu.edu.cn).

1 Introduction

As a symbol of urban underground space development, the construction of underground passages has been accelerating, with the shield method emerging as the preferred construction technique [1]. Two-line shield tunnels have become increasingly favored for urban underground passages in large cities due to their advantages, including better control of soil movement and internal forces in the lining [2].

Advances in shield machine technology now allow tunneling in a variety of environments, such as mudstone areas [1], shallow loess [3], marine clay layers [4], and shallow buried shield tunnels in sandy soils [5]. To optimize land use and support low-carbon urbanization, most urban underpass constructions now feature small-clearance tunnels [6]. Consequently, the interaction between closely spaced twin tunnels has become a significant focus in tunnel engineering [7].

Numerous scholars have studied the construction process of small-clearance tunnels and shield tunnels, covering topics such as numerical simulations of lining structures [8,9], analysis of settlement monitoring data [10–13], the impact of tunnel construction on existing buildings [14–16], analysis of the impact of ground settlement near the tunnel on the construction of pile foundations [17,18], and improvements to numerical models of tunnel structures [19–22]. Among these, numerical simulation methods are the most widely used in tunnel construction research. For example, Wu et al. [23] used Midas Geo-Technical Analysis System (GTS) finite element analysis software to study the effects of various excavation sequences and methods on tunnel stability, revealing the deformation and force characteristics of the tunnel. Cao et al. [24] analyzed stress distribution in characteristic sections and tunnel profiles using ground investigation data and numerical analysis software, identifying surrounding rock stress distribution areas and recommending treatment measures. Gao et al. [25] employed FLAC 3D numerical simulation software to study the stability of a large-scale traffic tunnel cluster in densely populated areas, proposing construction risk control techniques based on experimental scale model tests. Jiang et al. [26] compared and analyzed the deformation of surrounding rock under three tunnel excavation methods—beach cutting, center diaphragm (CD) method, and double-sided boring—using numerical simulations, and provided recommendations for method selection based on the actual project.

In recent years, research on small-clearance tunnels in urban soft soil areas has become increasingly common [27,28]. Existing studies on twin-shield tunnel construction have made significant progress in experimental modeling and theoretical analysis, providing strong technical support for the development of small clear distance tunnels. However, current research still lacks a systematic approach to evaluating shield advancement distances and analyzing surface settlement induced by continuous tunneling. This issue is particularly prominent in the context of riverbed tunnel construction, where there is still no unified theoretical framework to describe the spatiotemporal evolution of ground settlement. As a result, research findings often appear fragmented and lack generalizability. Although the finite element method (FEM) has been widely adopted as an auxiliary analytical tool, its potential for independent modeling and analysis remains underexplored—especially under complex hydrogeological and boundary conditions, where simulations tend to be limited to single-case scenarios. Therefore, it is of both theoretical and practical significance to develop independent FEM-based modeling strategies for systematically assessing ground settlement behavior under varying design conditions.

In response to this need, this paper focuses on the small-clearance, double-lane shield tunnel crossing the river in an urban setting. Using finite element software, three-dimensional modeling and phased simulations are conducted to realistically replicate the shield construction process in a soft

soil layer. The study systematically analyzes the temporal and spatial distribution of soil settlement patterns around the small-clearance tunnel, based on field data, and verifies the feasibility of the actual tunnel construction design.

2 Overview of Engineering Background

2.1 Project Overview

Heyan Road Crossing is a north-south tunnel that is completed and opened to traffic, located between Nanjing Yangtze River Bridge and Baguazhou Yangtze River Bridge. Tunnel excavation is carried out using a mud-water pneumatic balance shield machine. The machine has a total length of 140 m, with the main shield section measuring 14 m in length, and a cutter diameter of 15.03 m. The tunnel has a circular cross-section, and the structure uses the carriageway plate structure. The production of tube sheets and box culverts is carried out in the form of a combination of prefabricated road box culverts and cast-in-place reinforced concrete. The excavation section is shown in Fig. 1, divided into two tunnels on the left and right, both of which have a circular cross-section with a diameter of 13.90 m. The average distance between the centers of the two tunnels is 21.27 m, and the center of the tunnels is 16.25 m away from the ground surface. The tunnels pass through a river, and the section of the tunnel passing through the river is pre-filled with backfilled clay, pre-stressed reinforced concrete tubes, and reinforcing steel mesh. The tunnels are excavated in a parallel shield mode. To avoid excessive disturbance to the surrounding rock and soil layers, the right tunnel is excavated before the left tunnel, and the right tunnel is excavated for 20 m before the left tunnel is excavated. The two tunnels are excavated by a unified type of shield machine, which is 140 m long, and the subsequent segment material is C60 concrete. The segment is 2 m in length per ring, and it adopts universal wedge ring staggered seam assembling. The assembling speed of the segment before stopping the work for 21 days after excavation is 2 rings/day, and after resuming the work for 44 days after excavation, the assembling speed increases to 4 rings/day.

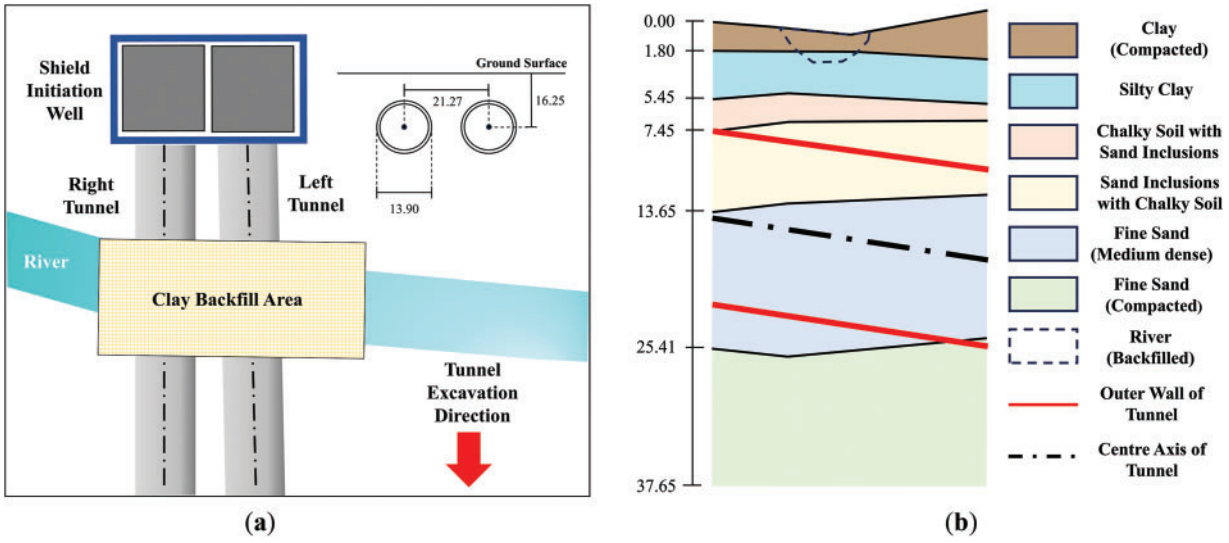

Figure 1: Construction area of shield tunnel (unit: m): (a) The plane relationship between the two tunnels of the first 100 rings of the tunnel; (b) Longitudinal geological profile of the interval tunnel

2.2 Geological and Hydrological Conditions

The terrain around the shield tunneling section is wide and the buildings have been demolished, the area for analysis is dominated by weak soil layers, the soil in the interval is specifically divided into six geotechnical layers, which are classified from top to bottom as clay, silty clay, heavily weathered pebbly sandstone (chalky soil with sand inclusions), sand inclusions with chalky soil, moderately dense fine sand, compacted fine sand, and the geotechnical layer profile is shown in Fig. 1b. All geomechanical parameters for the rock and soil layers are derived from *in-situ* core samples collected at the construction site and are obtained through laboratory geotechnical testing. Specifically, the elastic modulus and Poisson's ratio are determined via uniaxial compression tests; the unit weight is measured using the ring-shear method; and both cohesion and the internal friction angle are obtained from direct shear tests. Detailed geomechanical parameters for each layer are listed in Table 1, while the geological profile of the monitoring section—covering the riverbanks and a 10-m fill zone—is presented in Fig. 2. According to the regional data and regional construction experience, the water volume and head of this layer are high, so it is prone to engineering accidents such as surge and uplift of shield tunnel tubes.

Table 1: Physical properties of rock and soil

Material	Elasticity modulus (kN/m^2)	Poisson's ratio	Volume-weight (kN/m^3)	Cohesive force (kPa)	Frictional angle (°)
Clay (Compacted)	4420	0.35	18.1	25.2	8
Silty clay	4100	0.30	16.8	13.7	2
Chalky soil with sand inclusions	4600	0.30	19.2	24.5	7
Sand inclusions with chalky soil	5200	0.42	18.3	25.3	16
Fine sand (Medium dense)	12,930	0.25	19.4	5.1	35
Fine sand (Compacted)	15,000	0.25	20.8	10.1	36

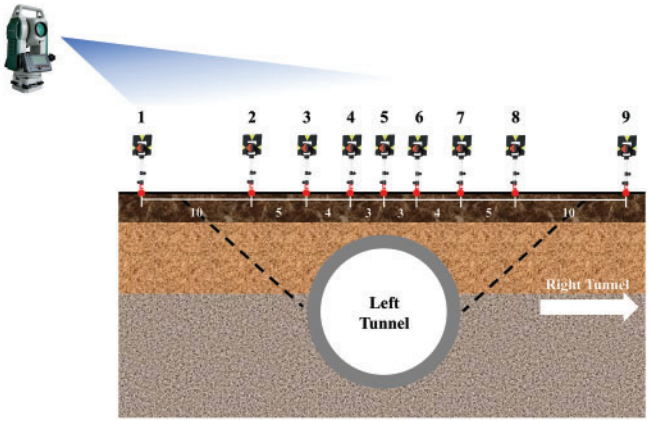

Figure 2: The surface settlement monitoring points in the section are arranged in cross-section (unit: m)

2.3 Content and Layout of Site Monitoring

Surface settlement point (SSP) will be arranged in this section. The content and arrangement of on-site monitoring will be based on the site conditions, and considering the convenience and accuracy of monitoring, the on-site monitoring point will be arranged at a distance of 16 rings from the starting point of the tunnel shield.

The lateral arrangement of the measurement points in the section is carried out in the way of Fig. 2 and is arranged according to 9 measurement points. Among them, the measurement point numbered 5 in the section is located near the center line of the left tunnel, the rest of the measurement points are symmetrically spread to both sides, and the measurement points numbered 7–9 cover the area between the two tunnels.

The monitoring program started after the start of the shield. When the excavation surface is less than 20 m from the front and back of the measurement section, the monitoring frequency will be once a day; when the excavation surface is more than 20 m from the front and back of the measurement section, the monitoring frequency will be once every two days; the observation will be finished after the completion of 60 rings of tunneling on the right line. The total number of on-site monitoring will be no less than 50 measurements to obtain more complete data for analysis. In response to significant changes in environmental conditions, such as heavy rainfall, the observation frequency will be adjusted to isolate the effects of these factors. Specifically, the monitoring frequency will be increased to twice the original rate. When the excavation surface is within 20 m of the measurement section, observations will be conducted twice daily. Conversely, when the excavation surface exceeds 20 m from the measurement section, the monitoring frequency will be adjusted to once daily.

3 Finite Element Analysis of Shield Tunnels

3.1 Model Establishment and Construction Condition Design

Finite element simulation analyses will be carried out using the geotechnical finite element software Midas GTS, and the left tunnel section ZK4+620∼ZK4+679 and the right tunnel section YK4+635∼YK4+694 (60 m in length) will be selected as the objects for the research. Fig. 3 illustrates the model dimensions. The research area has a length equal to 3.6 times the combined diameters of the two tunnels and a height equal to 2.7 times the tunnel diameter. Preliminary computations indicate that no abnormal settlement values appear in the boundary elements, which is consistent with the predictions of St. Venant's principle. Therefore, the influence of boundary effects can be effectively eliminated, affirming the appropriateness of the model boundary configuration.

The soil behavior is modeled using the Mohr-Coulomb criterion and segmented into six layers based on actual field conditions. The fundamental geomechanical parameters for each soil layer are derived from measured data (see Table 1), while the remaining parameters are adopted using the software's default settings. The grid side length of the model outside the tunnel excavation surface is 2 m, and the grid side length of the model inside the excavation surface is 1 m, and the parameters of the structural model for excavation calculation are set as shown in Table 2.

Based on the grid sensitivity analysis results presented in Tables 3 and 4, it is observed that the computational outcomes stabilized when the overall model comprised approximately 84,000 units, and the excavated soil surrounding both tunnels contains around 23,000 units. Consequently, the finite element model employed in this study is configured with a total of 84,372 units, of which 23,521 units are allocated to the excavated soil regions.

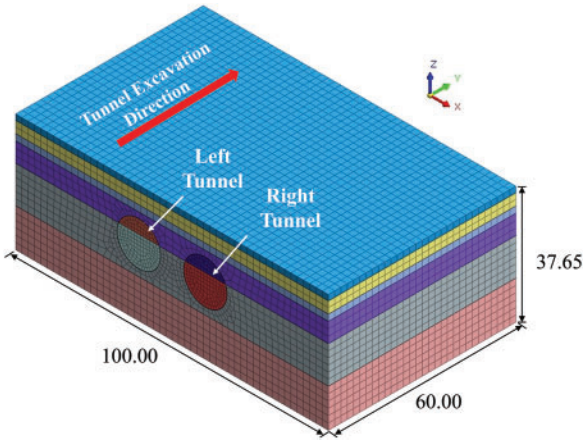

Figure 3: Diorama of the tunnel (unit: m)

Table 2: Mechanical properties of materials for numerical modelling

Structure name	Unit type	Constitutive model	Material used	Section shape	Section size
Soil layer 1	3D solid	Mohr-coulomb	Clay (Compacted)	–	–
Soil layer 2			Silty clay	–	–
Soil layer 3			Chalky soil with sand inclusions	–	–
Soil layer 4			Sand inclusions with chalky soil	–	–
Soil layer 5			Fine sand (Medium dense)	–	–
Soil layer 6			Fine sand (Compacted)	–	–
Shield machine	2D board unit	Elasticity	Steel Q345[1]	Board	Thickness 0.4 m
Segment			Concrete C60[2]		Thickness 0.6 m

Note: [1]The standard elastic modulus of Steel Q345 is 206 GPa; [2]The standard elastic modulus of Concrete C60 is 36.5 GPa.

Table 3: Grid sensitivity analysis for the overall finite element model

Serial number	Number of grid units	Stress value (MPa)	Rate of change (%)
1	76,830	792.2	−7.82
2	80,384	820.8	−4.49
3	84,259	859.4	–
4	86,432	872.2	1.49
5	88,190	876.1	1.94

Table 4: Grid sensitivity analysis for the excavated soil surrounding the tunnel

Serial number	Number of grid units	Stress value (MPa)	Rate of change (%)
1	19,833	698.3	−8.13
2	21,577	729.0	−4.09
3	23,498	760.1	–
4	27,843	768.2	1.07
5	29,014	769.5	1.24

The model adopts the solution type of the construction stage to restore and simulate the tunnel construction process in steps. The calculation process includes five construction phases, namely: geostress equilibrium, right tunnel starting, simultaneous excavation on both sides, installing the segment of right tunnel, and simultaneous installation of segments, and the specific added steps are shown in Table 5. In particular, during the initial geostress equilibrium stage, the stress history of each soil layer prior to tunnel excavation is simulated by applying the self-weight load to the entire model and imposing boundary constraints in both the excavation and horizontal directions.

Table 5: Construction phase steps

Serial number	Phase name	Phase type	Activated data	Passivated data
1	Geostress equilibrium*	Stress	Soil layers 1–6, deadweight loading, boundary constraints	–
2	Right tunnel starting		Shield machine of the right tunnel	Soil in the right tunnel
3	Simultaneous excavation on both sides		All shield machines	Soil in all tunnels
4	Install the segment of the right tunnel		Segments of the right tunnel	Shield machine of the right tunnelAP
5	Simultaneous installation of segments		All segments	All shield machines

Note: *When the ground stress is balanced, the displacement is set to 0 mm, and the water pressure is automatically considered.

To test the reasonableness of the design of the number of rings ahead of the right line tunnel construction, three kinds of synchronous construction conditions, namely, 4 rings ahead, 10 rings ahead and 16 rings ahead, will be designed by using finite element software and simulated construction simulation will be carried out, respectively. At the same time, to simulate the impact of the shield machine's self-weight, set the shield machine all covered by Q345 steel, and postpone the laying of segments during construction until after the shield machine has passed through all. The whole tunnel excavation is divided into 65 phases, each of which represents 1 day of the real construction period. Among them, according to the changes in the real working conditions and regulatory arrangements, the 22nd–43rd day of excavation is set as the shutdown phase. When the stoppage day arrives, if the left

and right shields have passed through the study area completely, the work will be stopped as scheduled; otherwise, the simultaneous work continues until the left-lane tunnel shield passes through the study area. The construction will be resumed on the 44th day of excavation in both cases.

To further assess the precision of the finite element model, a scenario in which the right tunnel leads the left by 10 rings is simulated in advance. Upon simulation completion, the lateral settlement values at observation nodes corresponding to the stabilized stage of soil settlement are extracted and compared with field measurements at the same time points, as presented in Fig. 4. The trend exhibited by the finite element results closely matches that of the measured data, and the magnitudes are of the same order, thereby demonstrating the reliability of the adopted modeling approach.

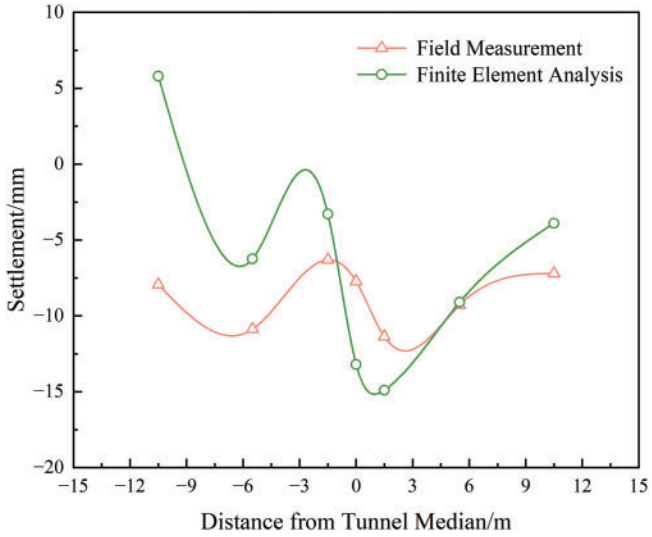

Figure 4: Comparison of lateral settlement values between finite element analysis and measured data on the 48th day of tunnel excavation (unit: mm)

3.2 Vertical Settlement Analysis

Three finite element nodes corresponding to the surface above the center line of the left tunnel, the surface above the overall center line of the small-clearance tunnel, and the surface above the center line of the right tunnel are extracted from the model, and the Z-direction vertical displacements of the finite element analysis results are selected for post-processing, and the calculation line diagrams for the three conditions are shown in Fig. 5.

Finite element analyses are conducted under three different working conditions to investigate longitudinal settlement behavior. The resulting displacement curves from these simulations exhibited consistent trends and closely match the conventional settlement curves derived from the modified Mindlin formula [29], i.e., the surface settlement above the left tunnel, the center tunnel, and the right tunnel all increased substantially shortly after tunnel excavation and peaked shortly after the arrival of the shield machine at the measurement point directly below the respective tunnel, after which the soil rebounded and finished rebounding 2 days after the project was shut down. The soil settlement remained constant as the shields passed completely through the model. A small increase in settlement was observed at the start of the segment installation, followed by soil rebound again until all segments were installed in the model.

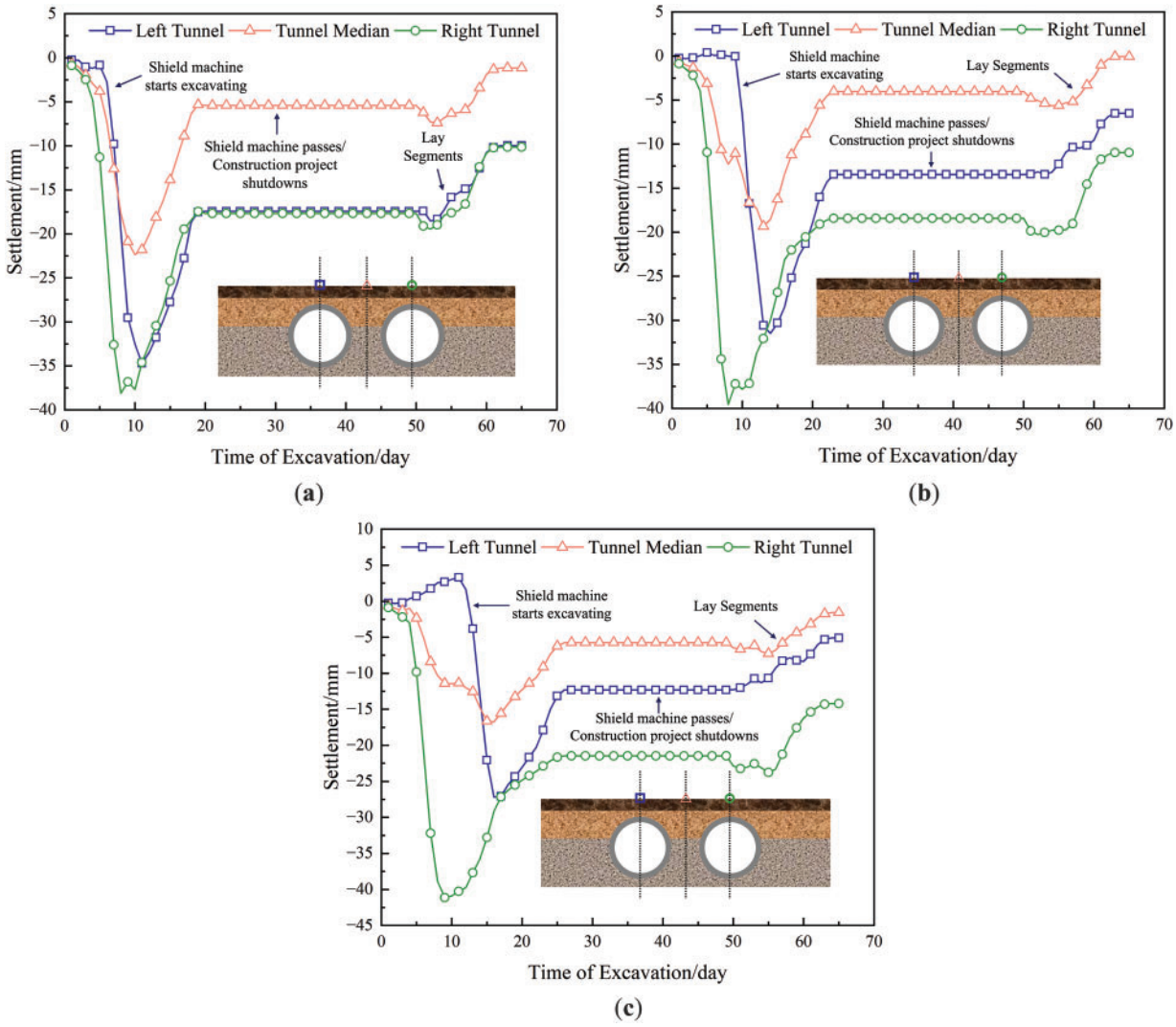

Figure 5: Vertical settlement during tunnel excavation under different construction conditions (unit: mm): (a) Leading 4 rings; (b) Leading 10 rings; (c) Leading 16 rings

Taking the case where the right tunnel leads the left by 4 rings as an example, the oversized excavation diameters of both tunnels induced substantial ground loss, and all 3 nodes experienced pronounced settlement immediately following excavation. The settlement of the right tunnel peaks on the 8th day after excavation, with a settlement of 38.11 mm; the settlement of the left tunnel peaks on the 11th day after excavation, with a settlement of 34.71 mm; and the settlement above the center line of the tunnel peaks on the 10th day after excavation, with a settlement of 22.37 mm. Influenced by the rebound of the uppermost layer of compacted clay, with the steel structure of the left and right shield machines passing through one after the other, the settlement of the right tunnel rebounds to 46% of its peak, the left tunnel settlement rebounds to 50% of its peak, and the settlement above the center line of the tunnel rebounds to 24% of its peak. On the 51st day of excavation, all nodes start to show the phenomenon of settlement and rebound first. On the 65th day of excavation, the settlement of the right leading tunnel decreases to 27% of the peak value, the settlement of the left lagging tunnel

decreases to 29% of the peak value, and the settlement above the center line of the tunnel decreases to 5% of the peak.

The surface settlement trend of the leading 10 rings is approximately the same as that of the 4 rings, but there are several differences as follows: (1) the settlement of the left tunnel is delayed and the settlement during the shutdown period is 77% of that of the leading 4 rings, which is presumed to be due to the increase in the leading construction distance, which results in the decrease of the disturbance of the first tunnel on the later tunnels; (2) the maximum settlement of the right tunnel in the leading 10 rings condition is 104% of that of the leading 4 rings, and the tunnel center line The maximum settlement is 86% of the leading 4 rings, and the maximum settlement of the left tunnel is 91% of the leading 4 rings.

The surface settlement trend of the leading 16 rings is approximately the same as that of the leading 4 rings, but there are several differences as follows: (1) the settlement time of the left tunnel is delayed, the surface bulge occurs on the 12th day after excavation, and the settlement during the shutdown period is 71% of that of the leading 4 rings, which is presumed to be due to the long leading construction distance, resulting in a weak disturbance effect of the first tunnel on the later tunnels; (2) the maximum settlement in the right tunnel under the working condition of the leading 16 rings is 108% of the leading 4 rings condition, the maximum settlement above the tunnel median is 75% of the leading 4 rings condition, and the maximum settlement above the left tunnel is 78% of the leading 4 rings condition.

Compared with the finite element data of the leading 10 rings of actual construction, the settlement of the left tunnel data of the leading 4 rings is larger, and the time point of sinking is advanced, which can easily lead to the difficulty of grouting and reinforcing the soil around the actual construction. The settlement of the left side tunnel data during pre-excavation and shutdown of the data of leading 16 rings is reduced by 4–8 mm relative to the data of the leading 10 rings, but the settlement of the right tunnel data during pre-excavation and shutdown of the tunnel is increased by 4–7 mm relative to the data of the leading 10 rings, and the maximum settlement is more than 40 mm, which is far more than the construction standard of 30 mm. Therefore, combining all finite element calculation results, the working condition of the leading 10 rings appears more feasible and carries relatively lower construction risk. However, since the maximum settlement exceeds the 30 mm standard and the settlement increase rate surpasses 3 mm/day, some risk persists. It is thus recommended that timely reinforcement measures be implemented in the surrounding area after tunnel excavation.

3.3 Lateral Settlement Analysis

Extract the cross-section that is 32 m away from the starting point in the finite element model and coincides with the measured point, and select the Z-direction vertical displacement of the finite element analysis results for post-processing, the calculation of the three conditions is shown in Fig. 6, and each condition will be based on the excavation distance of the first tunnel to select the observation time point, and the design of the selected time point is shown in Table 6. Because the shield machine in just excavated within 10 m, the finite element calculation results are not more than 5 mm, settlement distinction is not obvious, so the three conditions in the shield machine did not reach the observation surface, a unified selection of excavation 24 m time point data for analysis.

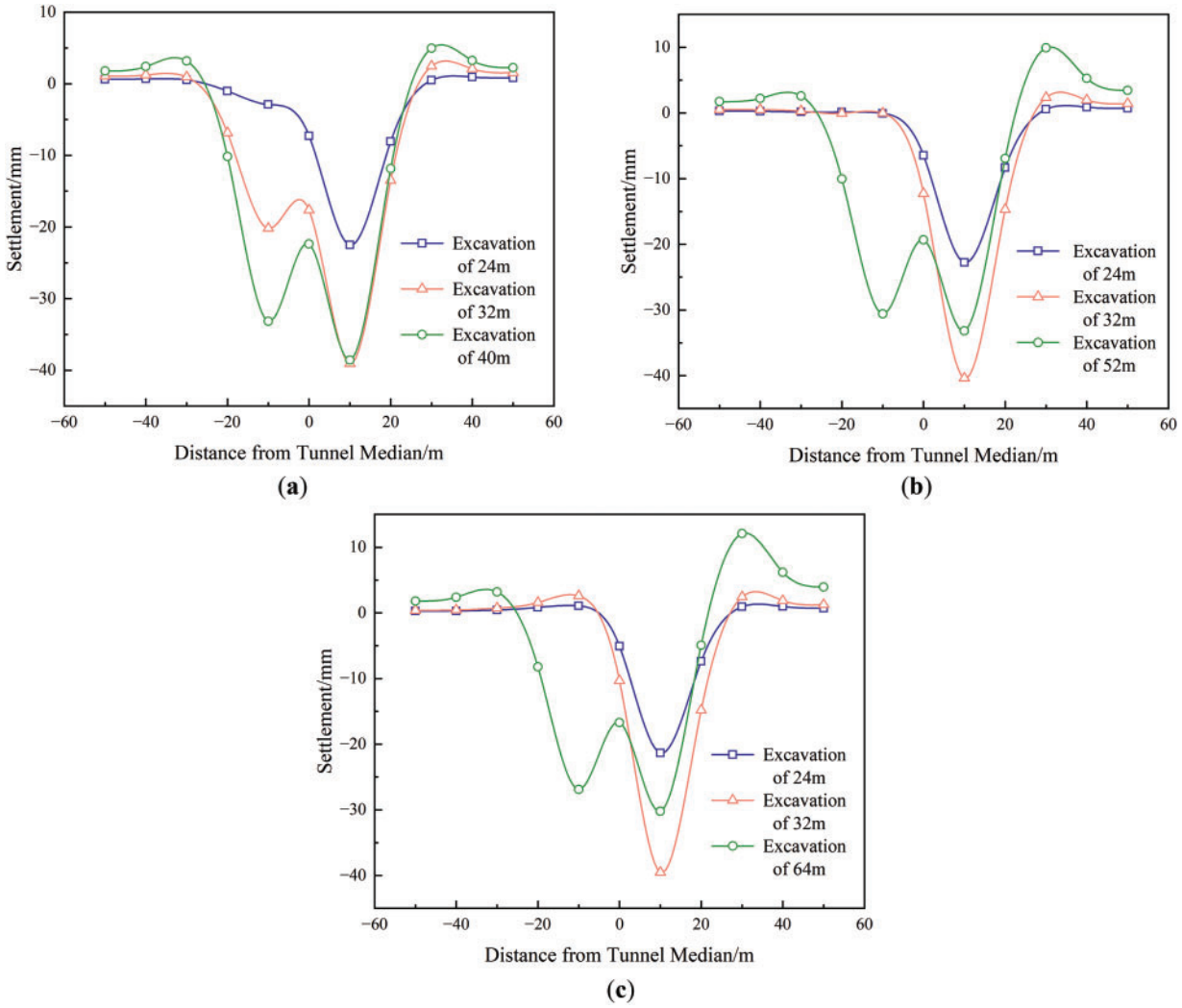

Figure 6: Lateral settlement during tunnel excavation under different construction conditions (unit: mm): (a) Leading 4 rings; (b) Leading 10 rings; (c) Leading 16 rings

Table 6: Selection of lateral settlement data

Construction condition	Selected time point (Distance of Right Tunnel Excavation)	Corresponding position
Leading 4 rings	24 m/32 m/40 m	The right shield machine is 8 m away from the cross section where the monitoring point is located
Leading 10 rings	24 m/32 m/52 m	The right shield machine arrives at the section where the monitoring point is located

(Continued)

Table 6 (continued)

Construction condition	Selected time point (Distance of Right Tunnel Excavation)	Corresponding position
Leading 16 rings	24 m/32 m/64 m	The left shield machine arrives at the section where the monitoring point is located

A total of 10 surface nodes are analyzed at 10 m intervals by selecting the actual lateral settlement observation cross-section corresponding to the model location. Taking the data of the leading 4 rings as an example, when the right leading tunnel is excavated for 24 m, funnel-like settlement occurs with the center line of the right tunnel as the center, and the maximum settlement of 22.51 mm is located right above the right tunnel. Under the influence of the excavation of the left backward tunnel, the left tunnel starts to settle right above it, and the amount of settlement is 2.9 mm. The nodes 30 m away from the center line of the tunnel and farther away do not show much change in the settlement. When the right leading tunnel is excavated for 32 m, the left and right tunnels both show funnel-like settlement. The settlement above the left tunnel is 20.19 mm, and the settlement funnel of the right tunnel is further extended downward, with the settlement above it being 39.07 mm. The nodes 30 m from the center line of the tunnel and farther away show soil bulging, with the maximum bulging amount of 2.46 mm, located on the right side of the right leading tunnel at a distance of 20 m. At 40 m of excavation of the right leading tunnel, the funnel-like settlement of the left and right tunnels is fully formed, with 33.16 mm of settlement above the left tunnel, and a slight convergence of the settlement funnel of the right tunnel, with 38.57 mm of settlement above the funnel. The nodal soil bulge 30 m from the center lines of the tunnels and beyond increases further, with a maximum bulge of 4.98 mm, located 20 m to the right of the right leading tunnel.

The surface settlement curve characteristics of the data of the leading 10 rings are similar to those of the leading 4 rings, but there are the following differences: (1) when the leading tunnel is excavated for 24 m, there is not much change in the settlement of the nodes directly above the left tunnel and 30 m and further away from the center line of the tunnel, which is presumed to be due to the increase of the leading construction distance, resulting in the decrease of the disturbance of the leading tunnel to the lagging tunnel; (2) when the leading tunnel is excavated for 32 m, the peak settlement of the right tunnel is 103% of that of the leading 4 rings, at 52 m of advance tunnel excavation, there is a significant convergence of the settlement funnel of the right tunnel, and the settlement above it decreases to 82% of its peak, which is 86% of the settlement value of the leading 4 rings, and the peak value of the soil augmentation at the nodes 30 m from the center line of the tunnel and beyond is 199% of that of the leading 4 rings and is located at the same position.

The surface settlement profile characteristics of the data of the leading 16 rings are similar to those of the leading 10 rings, with the peak settlement of the right tunnel being 101% of that of the leading 4 rings at 32 m of leading tunnel excavation, and the settlement above the right tunnel dropping to 76% of its peak at 64 m of advance tunnel excavation, which is 78% of the settlement value of the leading 4 rings, and the peak soil augmentation at the nodes 30 m from the center line of the tunnel and beyond being 243% of that of the leading 4 rings, which is located at the same location.

Comparing all the analysis results in Fig. 6, it can be seen that the finite element analysis results are consistent with the double funnel-shaped Peck curve of two-lane tunnel construction [30], and the nodes 30 m away from the center line of the tunnel and further away from the tunnel rebound after excavation, and the rest of the nodes show larger settlement, which is in line with the settlement law of the soil body. From the settlement maximum value of the right tunnel is larger than that of the left tunnel, it can be seen that the construction of the right tunnel is affected by the disturbance of the left tunnel, and the comparison of the final settlement curves of the right and left tunnels under different working conditions, as well as the rebound amount of the settlement of the right tunnel at the later stage, it can be seen that the closer the distance between the excavation surfaces is, the greater the disturbance is.

Compared to the finite element data for the actual construction of the leading 10 rings, the soil bulge on both sides of the tunnel in the leading 4 rings condition is smaller, but the settlement of its leading tunnel after the shield machine passes through the study area is larger, which results in higher risk for subsequent construction. Although the overall settlement characteristics of the case of the leading 16 rings are similar to that of the leading 10 rings, the soil on the right side of the advance tunnel, when the lagging tunnel arrives, bulges more than the 10 mm construction requirement. Therefore, all the finite element calculation results show that the condition of the leading 10 rings is more feasible, and the construction risk is relatively smaller.

4 Measured Analysis of Ground Settlement

The measured vertical cumulative settlement and lateral settlement data are shown in Fig. 7. Because in the actual measurement, measurement point 5 is located near the center line of the left tunnel, measurement point 8 is located near the overall center line of the small clear distance tunnel, and measurement point 9 is located near the center line of the right tunnel, the above three measurement points are selected to focus on the vertical settlement analysis. Field measurements indicate that the vertical ground settlement induced by the actual construction follows a typical pattern of initial subsidence followed by rebound, which closely resembles the conventional settlement curve derived from the Mindlin equation. In the lateral direction, the settlement profile exhibits a double-peak shape, consistent with the characteristics of the Peck curve. Overall, both the longitudinal and transverse settlement trends observed in the field align with the results of the finite element analysis.

4.1 Vertical Settlement Analysis

The overall pattern of vertical settlement along the tunnel centerline and directly above both the left and right tunnels is essentially identical, as illustrated in Fig. 7a. The cumulative settlement of the left tunnel gradually increases during the period from tunnel excavation starting to 21 days of excavation, with an average increase in settlement of 0.23 mm/day up to the time of shutdown, with a cumulative settlement of no more than 8 mm. During the period of project shutdown from 22 days of excavation to 43 days of excavation, the left tunnel slowly rebounds to 66% of the settlement before the shutdown. After the project resumed on the 44th day of excavation, the settlement begins to increase significantly, with an average increase in settlement of 0.52 mm/day from 44 days to 53 days, and an average increase in settlement of 2.1 mm/day from 53 days to 58 days, but it still meets the requirement that the daily increase in settlement for on-site construction should be no more than 3 mm, and the cumulative settlement should be no more than 30 mm.

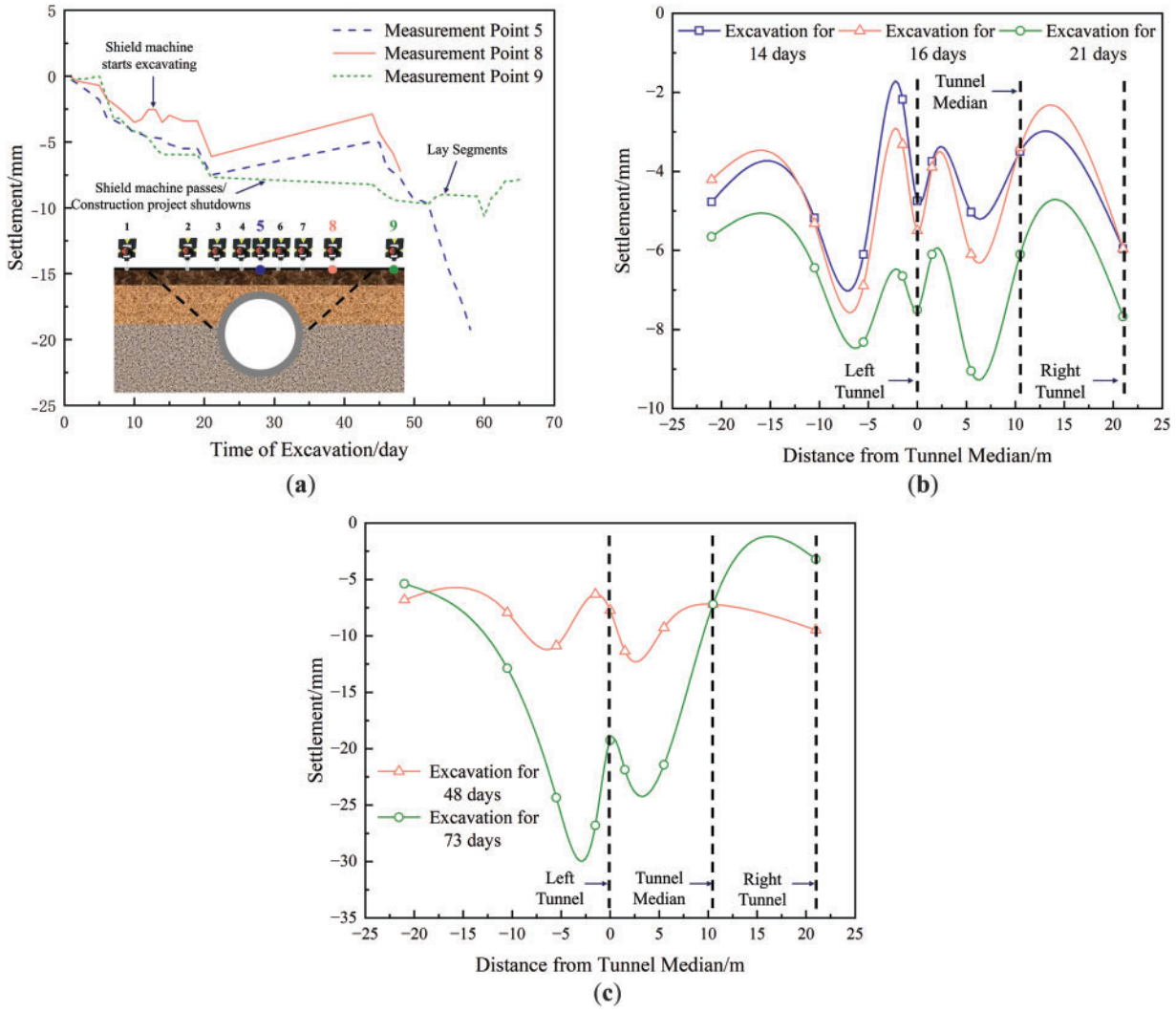

Figure 7: Measured settlements in different periods of tunnel excavation (unit: mm): (a) Vertical settlement at each major measurement point; (b) Lateral settlement (pre-construction period); (c) Lateral settlement (late construction period)

The overall settlement characteristics along the tunnel centerline are essentially similar to those of the left tunnel, although its daily settlement is lower. The average settlement increase of the middle line of the tunnel is 0.18 mm/day during 1–21 days of excavation, and the cumulative settlement does not exceed 6 mm. The settlement of the middle line of the tunnel slowly rebounds to 47% before the stoppage after 22–43 days of excavation. From 44 days of excavation to 48 days of stopping the observation, the average settlement increase is 0.57 mm/day, which meets the requirement that the settlement increase speed of site construction does not exceed 3 mm/day.

During the first 21 days of excavation, the right tunnel exhibits settlement increment characteristics that are essentially similar to those of the left tunnel. The difference is that, due to the leading construction, the surface of the right tunnel with the excavation 22–43 days of the project stoppage period appears to be slow settlement, and the increase in settlement does not exceed 0.1 mm/day, and

during the period of 44–65 days of the excavation, the surface above the tunnel shows the characteristics of first settlement and then rebound, in which the rate of increase in settlement from 44–52 days of the excavation is 0.17 mm/day, and in which the rate of rebound from 60–65 days of the excavation is 0.55 mm/day. During the construction of the right tunnel, the settlement increase is no more than 3 mm/day, and the rebound is no more than 2 mm/day, which are in line with the site construction requirements.

Unlike the finite element modeling scenario, in order to prevent the construction risk caused by excessive settlement, during the tunnel excavation to the stoppage period, the construction company carries out continuous and simultaneous grouting reinforcement treatment around the left and right sides of the shield machine passing through the area, which prevents the excessive settlement of more than 20 mm that appears in the finite element analysis. Under the influence of grouting, in the longitudinal settlement time series curve, the settlement of the three measurement points from 1 to 21 days of excavation shows a slow decreasing trend, and the daily increase in settlement does not exceed 0.3 mm/day, which is in line with the requirements of tunnel construction. In addition, measurement point 5 and measurement point 8 show accelerated settlement after the project resumes on 44 days of excavation. This is due to the accelerated subsidence of the ground surface caused by the pouring of the ground surface above the tunnel during the actual construction process.

4.2 Lateral Settlement Analysis

Lateral measured curve graphs are shown in Fig. 7b,c. On the 14th day of excavation, when the right tunnel is 2 rings away from the observed section, the overall settlement of the observed section is not more than 7 mm, and the overall settlement of the observed points 1–3 shows a gradual increase in the characteristics. The rate of change of the settlement gradually increases from left to right, and the settlement of the middle section of the observed points 3–5 and 5–7 shows a gradual decrease and then an increase in the characteristics, with the maximum settlement achieved at measurement point 3. The settlement at observation points 7–8 decreases, and the settlement at observation points 8–9 shows a gradual increase, with the rate of change of settlement gradually increasing from left to right, which is in line with the actual construction situation.

On the 16th day of excavation, when the right tunnel reaches the observation section, except for the slight rebound of measurement point 1, the overall settlement of the data of the rest of the observation points have increased, and the characteristics of the curve change are similar to that on the 14th day of excavation, in which the increase of the settlement of observation points 3, 4, 5 and 7 are all around 1 mm, and the maximum settlement is obtained at the measurement point 3, and the overall settlement of the observation section is not more than 7.5 mm.

On the 21st day of excavation, when the left tunnel reaches the observation section, the characteristics of the curve change are similar to those observed on the 14th and 16th days of excavation, and the overall settlement of the data at the observation points increases, of which the increase in settlement at the observation points 3, 5, and 6 increases to about 2 mm, and the increase in settlement at the observation points 4, 7, and 8 increases to about 3 mm, and the maximum settlement is obtained at the measurement point 7, and the overall settlement in the observation section does not exceed 10 mm.

Until the 48th day of excavation, when the observation of measurement point 8 is stopped, except for measurement points 5 and 9, where there is no change in settlement, the data of the other measurement points show an increase in the overall amount of settlement, among which measurement points 3 and 6 show more than 10 mm settlement, and the characteristics of the curve change remain essentially unchanged.

The last observation is made at all measurement points on the 73rd day of excavation. The data shows that there is a certain amount of soil rebound at measurement points 1 and 9, in which the soil rebound at measurement point 1 is 2.1 mm, and the soil rebound at measurement point 9 is more than 6 mm. There is no change in the settlement at measurement point 8, the settlement at measurement point 2 increases by 5 mm, and there is an increase in settlement of more than 10 mm at measurement points 3–7, in which the settlement at measurement point 4 increases by more than 20 mm. The characteristics of the curve change at 73 days of excavation are the same as at 48 days of excavation, with a maximum settlement close to 30 mm. Compared with the measurement data on the 48th day of excavation, the maximum surface settlement of the measurement data on the 73rd day of excavation increases by more than 20 mm, which is presumed to be caused by the accelerated surface subsidence due to the influence of the ground pouring construction on the surface near the observation point after resumption of work.

Due to the influence of the previous grouting work, the lateral settlement curves of the left tunnel, the center line of the tunnel, and the settlement curve near the measurement point directly above the right tunnel show obvious convergence, which is in line with the actual situation.

5 Discussion

The small clear distance tunnel, as a special form of twin tunnel design, features a narrow spacing between tunnel faces and high construction efficiency. It has thus been widely applied in urban transportation projects. However, compared to conventional twin tunnels, the construction of small clear distance tunnels is more susceptible to disturbances from adjacent tunnel excavation, leading to higher construction risks. Therefore, it is of great importance to investigate the ground surface settlement patterns caused by the construction of such tunnels and to validate the feasibility of the corresponding design approaches.

At present, ground surface settlement induced by shallow tunnel construction in soft soil layers is typically analyzed using the Mindlin integral solution. The most recent modified Mindlin formula [29] is expressed as follows:

$$\omega = \omega_q + \omega_f + \omega_v + \omega_P \tag{1}$$

where ω_q is the vertical ground displacement caused by the frontal thrust of the shield during the excavation and squeezing, ω_f is the vertical ground displacement caused by the softening of the soil and the friction of the unevenly distributed shield shell, ω_v is the vertical ground displacement caused by the ground losses, and ω_P is the vertical ground displacement caused by the simultaneous grouting pressure.

This study focuses on an actual small clear distance tunnel project as the research subject. By employing numerical simulation, the construction process was realistically replicated, and the temporal and spatial patterns of ground surface settlement during construction were obtained. Results from finite element analysis indicate that the settlement trends over time align well with the conventional settlement curves predicted by the modified Mindlin solution. Since the modified Mindlin formula incorporates factors such as excavation-induced ground loss, interface friction between the shield machine and surrounding soil, tail grouting pressure, and slurry pressure, it can be inferred that these factors also significantly influence settlement behavior in small clear distance tunnel construction.

In addition, based on the principle of displacement superposition in multi-line tunnel construction and the inverse correlation between settlement magnitude and distance as described in the Mindlin solution [31], it can be further inferred that ground settlement at a given point during small clear distance tunnel construction tends to be greater than that observed in conventional tunnel scenarios.

The settlement characteristics obtained in this study are consistent with those observed in other multi-line tunnel projects [32–35], in both vertical and lateral directions, thereby validating the reliability and applicability of the 3D finite element modeling approach adopted. However, compared with other projects, the small clear distance tunnel examined in this study exhibited faster settlement in the early stage, quicker rebound in the later stage, and higher peak settlement values due to stronger influences from spacing and construction disturbances. Owing to the adoption of temporary reinforcement measures similar to those used in other projects [36], the measured settlement curves in this study displayed a similar slow-settling trend.

Although the finite element analysis conducted in this study provides a relatively high degree of realism, some limitations remain. During the actual construction phase, surface hardening is accompanied by sand and rebar storage, as well as irregular movement of transport vehicles—conditions that are difficult to replicate accurately in the numerical model. As such, only the parameters of the topmost soil layers are adjusted, while detailed surface loading conditions are not included in the model. Furthermore, due to software limitations in simulating shield tunneling activities beyond the modeled area, some long-term settlement-affecting factors such as delayed ground loss [37] are omitted, leading to certain deviations in the rebound phase results.

Future research on small clear distance tunnel settlements should address these limitations by exploring optimized finite element modeling strategies, including the incorporation of dynamic loads. Additionally, considering the rapid development of settlement in such tunnels, it is essential to investigate integrated ground reinforcement techniques, such as ground freezing and temporary grouting, as well as their implementation in finite element models, to improve both prediction accuracy and design safety.

6 Conclusions

This research employed finite element modeling and analysis to simulate the construction process of the Heyan Road small clear distance tunnel, located within a soft soil layer. The simulation included various scenarios, such as shortening and lengthening the construction distance of successive tunnels. Additionally, the settlement patterns observed during the actual construction were analyzed, summarizing and comparing vertical and lateral settlement patterns from both finite element simulations and measured data. The key findings are as follows:

(1) The results of Finite Element Analysis demonstrate that the longitudinal settlement data for the leading 4-ring, 10-ring, and 16-ring construction stages align with the Mindlin settlement curves, while the transverse settlement data correspond to double-funnel Peck curves. When compared to the actual construction scenario of the leading 10-ring stage, the 4-ring stage exhibits a faster initial settlement rate and presents greater construction challenges. The 16-ring stage shows a peak settlement exceeding 40 mm and a peak bulge over 10 mm, both of which significantly surpass construction standards, making the 10-ring stage the most feasible option.

(2) Due to initial synchronous grouting reinforcement and the pouring of the floor above the tunnel, the measured data curves differ from the finite element results. During the first 21 days of excavation, the average longitudinal settlement rate at each measurement point did not exceed 0.3 mm/day, adhering to construction requirements. Between days 22 and 44, slight changes in settlement were observed at each measurement point. Subsequently, a significant increase in settlement was noted above the left tunnel and along the tunnel's centerline, affected by the surface pouring above the tunnel. However, this increase remained within the 30 mm settlement limit specified by construction requirements. The lateral settlement curve from the measured data closely aligns with

the double funnel-shaped Peck curve, exhibiting similar characteristics to those observed in the finite element analysis.

(3) Finite element analysis and field measurements consistently show that soil settlement in soft layers is strongly affected by construction activity, structural stiffness, lateral unloading, tube sheet weight, and shield machine movement. Therefore, in actual construction, it is recommended to install anti-floating anchors and perform synchronous grouting promptly to prevent excessive surface settlement.

Acknowledgement: The construction data used for the research, is provided by the China Railway Siyuan Survey and Design Group Co., Ltd. and China Design Group Co., Ltd.

Funding Statement: This research was funded by the Natural Science Foundation of Hunan Province of China, grant number No. 2024JJ8346; and the National Natural Science Foundation of China, grant number No. 42307193. The author, Shuangshuang Wu, received all the grants from the above institutions.

Author Contributions: The authors confirm contribution to the paper as follows: Conceptualization, Xun Zhao, Shuangshuang Wu, Fuyu Jiang and Song Chen; methodology, Xun Zhao, Shuangshuang Wu and Song Chen; software, Xun Zhao, Shuangshuang Wu, Fuyu Jiang and Song Chen; validation, Xun Zhao, Shuangshuang Wu and Song Chen; formal analysis, Xun Zhao, Shuangshuang Wu, Fuyu Jiang and Song Chen; investigation, Xun Zhao; resources, Xun Zhao, Shuangshuang Wu and Fuyu Jiang; data curation, Fuyu Jiang; writing—original draft preparation, Xun Zhao and Song Chen; writing—review and editing, Xun Zhao and Song Chen; visualization, Xun Zhao and Song Chen; supervision, Xun Zhao; project administration, Xun Zhao; funding acquisition, Xun Zhao and Shuangshuang Wu. All authors reviewed the results and approved the final version of the manuscript.

Availability of Data and Materials: The authors confirm that the data supporting the findings of this study are available within the article.

Ethics Approval: Not applicable.

Conflicts of Interest: The authors declare no conflicts of interest to report regarding the present study.

References

1. Yuan C, Zhang M, Ji S, Jin L. Analysis of factors influencing surface settlement during shield construction of a double-line tunnel in a mudstone area. Sci Rep. 2022;12(1):22606. doi:10.1038/s41598-022-27206-7.
2. Enieb M, Khalil AA, Ahmed ASH. Twin tunnel configuration for Greater Cairo metro line No. 4. Comput Geotech. 2015;68(2008):66–77. doi:10.1016/j.compgeo.2015.03.015.
3. Lei P, Han X, Tang J, Xia Y, Chai L, Liang X. Theoretical solutions for the vertical compressive stress of shallow neighbourhood loess tunnel foundation. J Asian Archit Build Eng. 2021;20(4):428–41. doi:10.1080/13467581.2020.1799799.
4. Chen J, Kang C, Shi Z. Displacement monitoring of parallel closely spaced highway shield tunnels in marine clay. Mar Georesources Geotechnol. 2015;33(1):45–50. doi:10.1080/1064119X.2013.784833.
5. Qiang S, Zhao L, Wang X, Li X, Wang F. Analysis of face stability for shallow shield tunnels in sand. Front Earth Sci. 2023;11:1287151. doi:10.32604/cmc.10.3389/feart.2023.1287151.

6. Guo H, Yuan D, Jin D, Ma Q, Zhao H. Theoretical analysis and numerical simulations for the safe clear distance of a shallow-buried twin-shield tunnel with small spacing. KSCE J Civ Eng. 2024;28(11):5277–89. doi:10.1007/s12205-024-2264-0.
7. Wang C, Liu X, Song D, Wang E, He Z, Tan R. Structural response of former tunnel in the construction of closely-spaced cross-river twin tunnels. Tunn Undergr Space Technol. 2024;147:105652. doi:10.1016/j.tust.2024.105652.
8. Zhang H, Hao Z, Ge Z, Zhang G, Chen S, Wang L. The construction mechanical behavior and deformation characteristics of lining structure: a case study of large-span and small-clearance tunnels. Structures. 2022;45:2007–21. doi:10.1016/j.istruc.2022.10.025.
9. Wang S, He X, Peng X, Wang Y, Li Z, Song Z. Influence of secondary lining thickness on mechanical behaviors of double-layer lining in large-diameter shield tunnels. Undergr Space. 2024;18(s2):130–50. doi:10.1016/j.undsp.2023.11.015.
10. Zhang X, Zhang C, Wang J. Effect of closely spaced twin tunnel construction beneath an existing subway station: a case study. J Test Eval. 2018;46(4):1559–73. doi:10.1520/JTE20160563.
11. Mei Y, Zhou D, Shi W, Zhang Y, Zhang Y. Laws and numerical analysis of surface deformation caused by excavation of large diameter slurry shield in upper-soft and lower-hard composite stratum. Buildings. 2022;12(9):1470. doi:10.3390/buildings12091470.
12. Zhang T, Li Z, Wang R, Zheng G, Lei H, Fan Q. Geostress-associated settlements of a raft-foundation building due to shield tunnelling in soft ground. Can Geotech J. 2024;62(3):1–12. doi:10.1139/cgj-2024-0010.
13. Yun J, Kim H, Yoo H. Three-dimensional modeling and analysis of ground settlement due to twin tunneling using GIS. Sustainability. 2024;16(14):5891. doi:10.3390/su16145891.
14. Zeng L, Zhang D, Lian C, Zhang J, Yin H. Study on the influence of an under-crossing parallel double-line shield tunnel on the existing tunnel structure. Mathematics. 2023;11(14):3125. doi:10.3390/math11143125.
15. Peng F, Ma S. Analysis of experimental data on the effect of double-line parallel shield tunneling on the deformation of adjacent buildings. Alex Eng J. 2021;60(4):3957–63. doi:10.1016/j.aej.2021.02.034.
16. Wei G, Guo B, Wang Z, Diao H, Wang X. Analysis of influence of deformation modes of retaining structures on deformation of a side shield tunnel. Sci Rep. 2022;12(1):19974. doi:10.1038/s41598-022-24534-6.
17. Soomro MA, Dai M, Cui ZD, Mangi N, Mangnejo DA, Zhao C. Impact of twin stacked tunnels on laterally loaded pile groups: an emphasis on settlement and load transfer mechanisms using centrifuge and numerical modelling. Structures. 2024;70(1):107746. doi:10.1016/j.istruc.2024.107746.
18. Lu H, Shi J, Shi C, Pei W, Chen S. Assessment of twin tunnelling induced settlement and load transfer mechanism of a single pile in dry sand. Can Geotech J. 2023;61(5):1004–17. doi:10.1139/cgj-2023-0196.
19. Yan Q, Yao C, Yang W, He C, Geng P. An improved numerical model of shield tunnel with double lining and its applications. Adv Mater Sci Eng. 2015;2015(1):430879. doi:10.1155/2015/430879.
20. Li S, Chen Y, Huang L, Guo E. Study on response and influencing factors of shield single/twin tunnel under seismic loading using FLAC 3D. Shock Vib. 2022;2022(1):2224198. doi:10.1155/2022/2224198.
21. Hu J, Chai S, Wang H, Chen J, Fu X, Zhou Y. Longitudinal mechanical properties of shield tunnels crossing soft and hard mutation strata. Int J Geomech. 2023;23(12):04023225. doi:10.1061/IJGNAI.GMENG-8608.
22. Zheng A, Huang F, Tang Z, He Z. Stability analysis of neighborhood tunnels with large section constructed in steeply jointed rock mass. Math Probl Eng. 2020;2020(1):9641291. doi:10.1155/2020/9641291.
23. Wu S, Wu J, Liu D. Research on construction sequences and construction methods of the small clear-distance, double-arch tunnel under an asymmetrical load. Appl Sci. 2023;13(14):8242. doi:10.3390/app13148242.
24. Cao S, Huo S, Guo A, Qin K, Xie Y, Meng Z. Numerical simulation research on the stability of urban underground interchange tunnel group. Math Probl Eng. 2021;2021(1):9913509. doi:10.1155/2021/9913509.
25. Gao X, Kong C, Wu D, Lu F, Liu M, Wang H, et al. Construction risk control technology of a large tunnel complex in urban area. Front Earth Sci. 2022;10:1079405. doi:10.3389/feart.2022.1079405.

26. Jiang Q, Song S, Li T, Wang K, Gu R. Study on surrounding rock stability of small clear-distance twin highway tunnel with eight lanes. Geotech Geol Eng. 2019;37(2):593–8. doi:10.1007/s10706-018-0629-1.
27. Do NA, Dias D. A comparison of 2D and 3D numerical simulations of tunnelling in soft soils. Environ Earth Sci. 2017;76(3):102. doi:10.1007/s12665-017-6425-z.
28. Wang Z, Feng W, Wu S, Wu P, Xu S, Yao Z, et al. Research on strata deformation induced by EPB tunneling in round gravel stratum and its control technology. Appl Sci. 2022;12(20):10553. doi:10.3390/app122010553.
29. Feng X, Wang P, Liu S, Wei H, Miao Y, Bu S. Mechanism and law analysis on ground settlement caused by shield excavation of small-radius curved tunnel. Rock Mech Rock Eng. 2022;55(6):3473–88. doi:10.1007/s00603-022-02819-6.
30. Islam MS, Iskander M. Twin tunnelling induced ground settlements: a review. Tunn Undergr Space Technol. 2021;110(3):103614. doi:10.1016/j.tust.2020.103614.
31. Shi C, Cao C, Lei M. An analysis of the ground deformation caused by shield tunnel construction combining an elastic half-space model and stochastic medium theory. KSCE J Civ Eng. 2017;21(5):1933–44. doi:10.1007/s12205-016-0804-y.
32. Shi X, Lai J, Ma C, He S, Li B, Liu T, et al. Soil disturbance effects of pile-reinforced metro foundation subjected by tunnelling beneath: field investigation and model tests. Structures. 2024;69(12):107280. doi:10.1016/j.istruc.2024.107280.
33. Yan B, Wang R, Wang Y. Deformation of adjacent buildings and ground settlement induced by shield construction of three-line small-spacing tunnels. Alex Eng J. 2023;79(4):237–51. doi:10.1016/j.aej.2023.08.022.
34. Zhu T, Huang F, Li S, Ouyang T, Ying J, Zhao H. Optimization of pre-grouting construction and evaluation of grouting effect in a deeply buried silt-filled shield tunnel. Tunn Undergr Space Technol. 2024;152:105902. doi:10.1016/j.tust.2024.105902.
35. Lou P, Li Y, Tang X, Lu S, Xiao H, Zhang Z. Influence of double-line large-slope shield tunneling on settlement of ground surface and mechanical properties of surrounding rock and segment. Alex Eng J. 2023;63(9):645–59. doi:10.1016/j.aej.2022.11.038.
36. Zhang Q, Zhang X, Wang H, Zhang X, Li F, Xu D. Ground deformation induced by a shallow-buried twin-tunnel with small spacing: a case study of Guangzhou Metro Line 18 excavated by earth-pressure balance TBM. Environ Earth Sci. 2023;82(12):297. doi:10.1007/s12665-023-10993-1.
37. Jin D, Shen X, Yuan D. Theoretical analysis of three-dimensional ground displacements induced by shield tunneling. Appl Math Model. 2020;79(8):85–105. doi:10.1016/j.apm.2019.10.014.